
Self Supervised Learning for Object Localisation in 3D Tomographic Images

Yaroslav Zharov*, Alexey Ershov, Tilo Baumbach
 Institute for Photon Science and Synchrotron Radiation
 Karlsruhe Institute of Technology

yaroslav.zharov@kit.edu, ershov@kit.edu, tilo.baumbach@kit.edu

Abstract

While a lot of work is dedicated to self-supervised learning, most of it is dealing with 2D images of natural scenes and objects. In this paper, we focus on *volumetric* images obtained by means of the X-Ray Computed Tomography (CT). We describe two pretext training tasks which are designed taking into account the specific properties of volumetric data. We propose two ways to transfer a trained network to the downstream task of object localization with a zero amount of manual markup. Despite its simplicity, the proposed method shows its applicability to practical tasks of object localization and data reduction.

1 Introduction

Self-supervised learning (SSL) is a popular technique which shows promising performance for a number of tasks and applications [Jing and Tian, 2020]. Many methods are aiming at a general-purpose representation learning [Noroozi and Favaro, 2016, Pathak et al., 2017, Jenni and Favaro, 2018]. Others can be used for object localization [Lee et al., 2019]. In most cases SSL techniques are applied to 2D photographic images representing natural scenes.

Computed tomography (CT) is an important technique for medical, material sciences and many industrial applications. The 3D tomographic data differs from the 2D photographic images in two important aspects. In photography, the projective geometry and varying imaging conditions substantially change the appearance of a scene, objects and their relations. While in CT the imaging conditions and data acquisition protocol are usually fixed throughout an experiment. This information can be exploited to devise a method, which relies on the specific 3D structure and features of object of interest. Additionally, the variability in appearance and positioning of background objects (e.g. sample holders, frames, tubes, etc) in CT data is much lower than in natural scenes.

In this paper, we propose to use structural differences between an object and a background to solve the task of object localization in a self-supervised manner. We will describe both pretext losses for the self-supervision and methods to transfer a trained network to the downstream localization task without any labels required.

In the experiments section, we show that the fitted estimator has to rely on structural features of an object. Thus, the designed task and proposed losses are well suited for representation learning. Moreover, the localization result could be useful for further downstream tasks (e.g. object alignment or weak supervision for semantic segmentation). Practically, the proposed approach could aid the task of data reduction, which is a crucial topic, since modern high-resolution or high-throughput CT scanners yield huge data rates.

*corresponding author

2 Method

In this section we will describe two losses for self-supervised training for the task of object localisation. We denote them as *sorting loss* and *rotation loss*. Both are designed under the assumption that the object of interest is less homogeneous and more structured than the background (see Figures 1 and 2 for intuition), but exploit this assumption differently.

We also describe two methods to employ the trained estimator to obtain predictions for object localisation. One method is based on superpixel *embeddings clustering* and another is based on *uncertainty estimation*. The first approach is more universal, but requires an additional training to solve a clustering task.

We will use the following notation throughout the paper. Each element of dataset $\mathcal{X}_{i=1}^N$ is a 3D volumetric image of arbitrary size. To avoid multiple indexing we will usually denote i -th element along the slicing axis of the 3D array as \mathbf{x}_i , which is a 2D image slice. We assume is selected with respect to conditions described for specific loss. We will denote the neural network as f_θ , where θ is a set of parameters being optimised. We will denote a batch of data of size bs as $\{x_i, y_i\}_{i=0}^{bs}$.

2.1 Pretext losses

Sorting loss The sorting loss is inspired by jigsaw puzzle task proposed by Noroozi and Favaro [2016] and requires the network to predict the order in a batch of randomly chosen slices. For this loss to enforce the object localisation, object should be less permutation invariant (i.e. order of slices is predictable by the object appearance) along the slicing axis than the background. Due to the random positioning of different objects along the slicing axis, it's important to estimate the loss function between the slices taken from the same volume. We define the following sampling procedure.

$$\eta_i \sim \mathcal{P}_\eta(l); \zeta = \text{argsort}(\eta); \{x_i = \mathbf{x}_{\eta_i}; y_i = \zeta_i\}_{i=0}^{bs} \quad (1)$$

, where $\mathcal{P}_\eta(l)$ defines the sampling procedure to get a slice.

To get a correct ordering, the optimisation should be performed using a variant of ranking loss. In this work we use pairwise *margin ranking* loss, which is defined as:

$$\mathcal{L}(\theta, x, y) = \sum_{i=0}^{bs} \sum_{j=0}^{bs} \max(0, -[y_i < y_j](f_\theta(x_i) - f_\theta(x_j)) + m) \quad (2)$$

, where m is arbitrary set margin.

As a control metric we propose to use a mean displacement, which we define as a mean absolute distance between the predicted order and the true order of slices: $\frac{1}{bs} \sum_i |y_i - \xi_i|; \xi = \text{argsort}(f_\theta(x))$.

Rotation loss The rotation loss requires from an estimator to predict an angle between two randomly rotated slices. To achieve this we use the pretext task proposed by Gidaris et al. [2018] and modify it taking into account the specifics of the CT data. For rotation loss to be effective and forcing the network to learn object-related features, an object should be less rotational symmetric than the background (compare left and right views on the figure 2 for intuition). To avoid overfitting to the features of noise and background objects, and artifacts of rotation we (1) use two different but closely spaced slices instead of rotating copies of the same slice and (2) cropping each slice with an incircled mask of maximal diameter to allow rotations other than 90 degree. It is worth noting, that during the optimisation of the rotational loss all rotation-based augmentations should be either excluded or synchronised across a pair of slices. We define the batch sampling procedure as follows:

$$\eta_i, \sigma_i, c_i \sim \mathcal{P}_\eta(l), \mathcal{P}_\sigma(s), \mathcal{U}(0, |A|); \alpha_i = A_{c_i}; \{x_i = (\mathbf{x}_{\eta_i}, r_{\alpha_i}(\mathbf{x}_{\eta_i + \sigma_i})); y_i = c_i\}_{i=0}^{bs} \quad (3)$$

, where A is a discrete, pre-defined table of possible rotation angles, r_α is a rotation by an angle of α degrees, and by the (\cdot, \cdot) we mean the concatenation of two images along the channel axis. $\mathcal{P}_\eta(l)$ denotes the distribution of the initial slices and $\mathcal{P}_\sigma(s)$ – the distribution of distances to the rotated slices.

As the loss function, any classification loss might be used. We selected the negative log-likelihood minimisation with the softmax scores normalisation.

2.2 Transfer methods

Embeddings clustering To implement this approach we again exploit the assumption that the object appearance is more diverse and structured than the one of a background. We propose to cluster the embeddings from the last layer of a trained network. If the features of an object are more relevant for the imposed task, the embeddings from that region should affect the decision of an estimator more than the ones from a background, which means they will have larger variation and magnitude. As a result, we can employ clustering methods to find dense clusters of similar superpixel embeddings to label them as a background.

Uncertainty estimation For the task of rotation estimation, we assume that an object is randomly oriented w.r.t background objects during the CT scanning procedure. Thus the appearance of an object does not correlate with the selection of a slicing axis. Our implementation replaces the *3D localisation* task with a series of *2D detection* tasks. We run a detection task for each slice on each of the orthogonal 3D axes. A slice is denoted to contain an object if the estimator prediction achieves a high degree of certainty. Bounding box coordinates accross particular axis is defined by thresholding these certainty estimations. We use prediction uncertainty of the network by checking the probability of the correct class. In principle, any other uncertainty estimation method could be used as an alternative to the proposed technique.

3 Experiments

To prove that our methods provide reasonable results we show one qualitative and one quantitative experiment. For the qualitative example, we use CT datasets of the *Medaka* fish scanned with the same procedure as described by Weinhardt et al. [2018]. For the quantitative example, we use CT datasets of *Xenopus Laevis* embryos scanned as described by Moosmann et al. [2013].

For all experiments we use PyTorch framework Paszke et al. [2019], with Adam [Kingma and Ba, 2015] as an optimizer. We selected the ResNet-50 architecture [He et al., 2016] for all experiments. We also make use of augmentations using Albumentations framework [Buslaev et al., 2020]. For clusterisation and linear classifier training we used Scikit-Learn library by Pedregosa et al. [2011]. Catalyst [Kolesnikov, 2018] and Weights and Biases [Biewald, 2020] were used for experiments setup and tracking.

3.1 *Medaka* fish experiment

We have selected 15 3D CT fish samples and randomly set 4 of them for the test set. All of the presented volumes were on average of a size of $6100 \times 2000 \times 2000$ pixels, differing a bit along the rotation axis due to the imaging procedure and sample size.

We trained a neural network with a sorting loss as the target loss and used the embeddings clustering as an exploration technique. We set $\mathcal{P}_\eta(l) = \mathcal{N}(\frac{l}{2}, \frac{l}{5})$ to avoid sampling in the empty area of the volume (close to borders). The margin was set to $m = 0.1$. In the localisation task we selected a DBSCAN clustering method [Ester et al., 1996] (with $\epsilon = 0.5$) for its ability to detect outliers. To make further predictions we train a linear classifier on the clusterisation results.

Since loss achieved 5×10^{-3} for both the train and the test set, we conclude that there was no overfitting on specific samples. Since the mean displacement reached 0.42 on the test set and 0.26 on the train set for the batch size of $bs = 12$, we conclude that the estimator have learned a meaningful ordering using structural information inside these samples. The linear classifier trained for prediction achieved 0.98 AUROC and therefore is a trustworthy replacement.

In Figure 1 we present an example of a localisation task for a *Medaka* fish sample. The quality of the estimated bounding box results was sufficient to drive an effective, lossless cropping procedure. It reduced the storage space on average for 78% per volume, i.e. from 24 Gb to 5 Gb.

3.2 *Xenopus Laevis* embryo experiment

We have selected 34 volumetric images of the *Xenopus Laevis* embryos on different stages of development and randomly set 9 of them as the test set. The dataset also contained ground truth

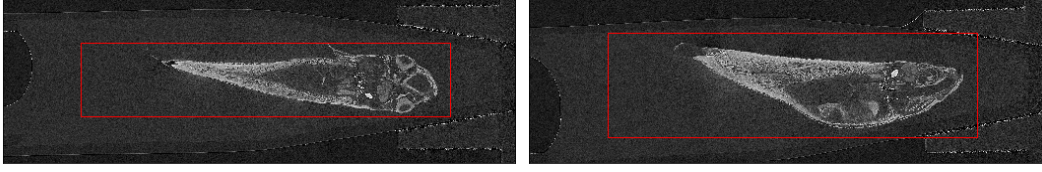


Figure 1: Predicted 3D bounding box for the *Medaka* fish dataset. Left: Coronal view. Right: Sagittal view.

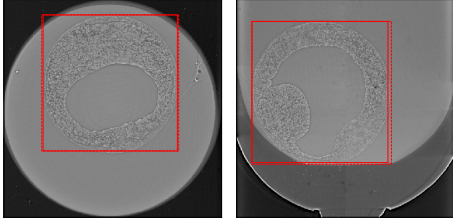


Figure 2: Predicted 3D bounding box for the *Xenopus Laevis* embryo depicted with a solid line and the ground truth depicted with a dashed line. Left: Axial view. Right: Coronal view.

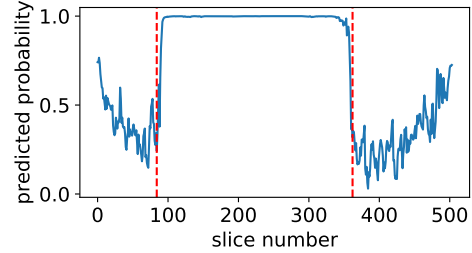


Figure 3: Probabilities of the correct class of 'object' for all slices along one slicing axis of *Xenopus Laevis* embryo. Ground truth position of the embryo shown with dashed red lines.

bounding boxes as labels selected by the expert. The original size of the presented volumes were $2000 \times 2000 \times 2000$ pixels, but for the training of a neural network they were downscaled to $512 \times 512 \times 512$ pixels.

We trained a neural network with the rotation loss and used uncertainty estimation approach to solve the localisation task. We set up $A = \{-90, -60, -30, 0, 30, 60, 90\}$ to be rotation labels. Also we selected $\mathcal{P}_\eta(l) = \mathcal{U}(0, l)$ and $\mathcal{P}_\sigma(s) = \mathcal{U}(-s, s); s = 100$.

As a sanity proof of the uncertainty estimation approach, we provide a plot of the predicted probabilities of the correct class along a single axis (See Figure 3). The area predicted to belong to the embryo have consistently higher probability than the area related to the background. We conclude that the neural network was trained to use intrinsic features of the embryo and not of the background to solve the rotation estimation task. The absolute error of bounding box coordinates averaged across all axes is 3.55 pixels. This is 1.2% taking into account the average size of an embryo of approximately 300 pixels across any axis. We also provide a qualitative bounding box in Figure 2.

4 Conclusion & Further work

In this paper we presented two ways of self-supervised learning suited for specificity of the *volumetric* X-ray CT data. We described two pretext tasks and respective loss functions and two ways to transfer the trained networks to a downstream task of object localisation with zero labeling.

In the experiments section, we back up our methods with both qualitative and quantitative analysis. Presented approaches show the ability to localise sample with 1.2% relative error and practically allows to shrink the used storage size by 78% by cropping the original 3D volume.

As a future work we plan to find additional pretext tasks and suitable losses to extend the described assumptions. We also plan to employ the proposed method to replace an expert-driven bounding box selection for such a popular task as the weak supervision for semantic segmentation [Hsu et al., 2019]. Additionally, we plan to provide a more comprehensive comparison of the presented method with the fully-supervised approaches, as well as in-depth ablation studies and experiments on open data. Clearly, as soon as these advanced studies would be done, we will open-source our code and all datasets.

Acknowledgments and Disclosure of Funding

We acknowledge the support by the projects CODE-VITA (BMBF; 05K2016) and HIGH-LIFE (BMBF; 05K2019). We thank Sabine Bremer for the provided *Medaka* fish samples and Janes Odar for the provided *Xenopus Laevis* samples. We acknowledge the KIT for provision of instruments at the Karlsruhe Research Accelerator (KARA) and thank the personnel of imaging beamlines.

References

- L. Biewald. Experiment Tracking with Weights & Biases, 2020. URL <https://www.wandb.com/>.
- A. Buslaev, V. I. Iglovikov, E. Khvedchenya, A. Parinov, M. Druzhinin, and A. A. Kalinin. Albu-mentations: Fast and flexible image augmentations. *Information (Switzerland)*, 11(2), 2020. ISSN 20782489. doi: 10.3390/info11020125.
- M. Ester, H.-P. Kriegel, J. Sander, and X. Xu. A Density-Based Algorithm for Discovering Clusters in Large Spatial Databases with Noise. In *Proceedings of the 2nd International Conference on Knowledge Discovery and Data Mining*, 1996.
- S. Gidaris, P. Singh, and N. Komodakis. Unsupervised representation learning by predicting image rotations. *6th International Conference on Learning Representations, ICLR 2018 - Conference Track Proceedings*, 3 2018. URL <http://arxiv.org/abs/1803.07728>.
- K. He, X. Zhang, S. Ren, and J. Sun. Deep residual learning for image recognition. In *Proceedings of the IEEE Computer Society Conference on Computer Vision and Pattern Recognition*, volume 2016-Decem, 2016. doi: 10.1109/CVPR.2016.90.
- C.-C. Hsu, K.-J. Hsu, C.-C. Tsai, Y.-Y. Lin, and Y.-Y. Chuang. Weakly Supervised Instance Segmentation using the Bounding Box Tightness Prior. In H. Wallach, H. Larochelle, A. Beygelzimer, F. dtextquotesingle Alché-Buc, E. Fox, and R. Garnett, editors, *Advances in Neural Information Processing Systems 32*, pages 6586–6597. Curran Associates, Inc., 2019. URL <http://papers.nips.cc/paper/8885-weakly-supervised-instance-segmentation-using-the-bounding-box-tightness-prior.pdf>.
- S. Jenni and P. Favaro. Self-Supervised Feature Learning by Learning to Spot Artifacts. *Proceedings of the IEEE Computer Society Conference on Computer Vision and Pattern Recognition*, pages 2733–2742, 6 2018. ISSN 10636919. doi: 10.1109/CVPR.2018.00289. URL <http://arxiv.org/abs/1806.05024>.
- L. Jing and Y. Tian. Self-supervised Visual Feature Learning with Deep Neural Networks: A Survey. *IEEE Transactions on Pattern Analysis and Machine Intelligence*, pages 1–1, 2 2020. ISSN 0162-8828. doi: 10.1109/tpami.2020.2992393. URL <http://arxiv.org/abs/1902.06162>.
- D. P. Kingma and J. L. Ba. Adam: A method for stochastic optimization. In *3rd International Conference on Learning Representations, ICLR 2015 - Conference Track Proceedings*, 2015.
- S. Kolesnikov. Accelerated deep learning R&D. \url{https://github.com/catalyst-team/catalyst}, 2018.
- W. Lee, J. Na, and G. Kim. Multi-task self-supervised object detection via recycling of bounding box annotations. In *Proceedings of the IEEE Computer Society Conference on Computer Vision and Pattern Recognition*, volume 2019-June, pages 4979–4988, 2019. ISBN 9781728132938. doi: 10.1109/CVPR.2019.00512.
- J. Moosmann, A. Ershov, V. Altapova, T. Baumbach, M. S. Prasad, C. LaBonne, X. Xiao, J. Kashef, and R. Hofmann. X-ray phase-contrast in vivo microtomography probes new aspects of *Xenopus* gastrulation. *Nature*, 497(7449):374–377, 5 2013. ISSN 0028-0836. doi: 10.1038/nature12116. URL <http://www.nature.com/articles/nature12116>.
- M. Noroozi and P. Favaro. Unsupervised learning of visual representations by solving jigsaw puzzles. *Lecture Notes in Computer Science (including subseries Lecture Notes in Artificial Intelligence and Lecture Notes in Bioinformatics)*, 9910 LNCS:69–84, 3 2016. ISSN 16113349. doi: 10.1007/978-3-319-46466-4_{5}. URL <http://arxiv.org/abs/1603.09246>.

- A. Paszke, S. Gross, F. Massa, A. Lerer, J. Bradbury, G. Chanan, T. Killeen, Z. Lin, N. Gimelshein, L. Antiga, A. Desmaison, A. Kopf, E. Yang, Z. DeVito, M. Raison, A. Tejani, S. Chilamkurthy, B. Steiner, L. Fang, J. Bai, and S. Chintala. PyTorch: An Imperative Style, High-Performance Deep Learning Library. In H. Wallach, H. Larochelle, A. Beygelzimer, F. d\textquotesingle Alché-Buc, E. Fox, and R. Garnett, editors, *Advances in Neural Information Processing Systems* 32, pages 8026–8037. Curran Associates, Inc., 2019. URL <http://papers.nips.cc/paper/9015-pytorch-an-imperative-style-high-performance-deep-learning-library.pdf>.
- D. Pathak, R. Girshick, P. Dollár, T. Darrell, and B. Hariharan. Learning features by watching objects move. *Proceedings - 30th IEEE Conference on Computer Vision and Pattern Recognition, CVPR 2017*, 2017-Janua:6024–6033, 12 2017. doi: 10.1109/CVPR.2017.638. URL <http://arxiv.org/abs/1612.06370>.
- F. Pedregosa, O. Grisel, R. Weiss, A. Passos, M. Brucher, G. Varoquax, A. Gramfort, V. Michel, B. Thirion, O. Grisel, M. Blondel, P. Prettenhofer, R. Weiss, V. Dubourg, and M. Brucher. Scikit-learn: Machine Learning in Python. *Journal of Machine Learning Research*, 12:2825–2830, 2011. ISSN 15324435.
- V. Weinhardt, R. Shkarin, T. Wernet, J. Wittbrodt, T. Baumbach, and F. Loosli. Quantitative morphometric analysis of adult teleost fish by X-ray computed tomography. *Scientific Reports*, 8 (1):16531, 12 2018. ISSN 2045-2322. doi: 10.1038/s41598-018-34848-z. URL <http://www.nature.com/articles/s41598-018-34848-z>.